A-Appendix

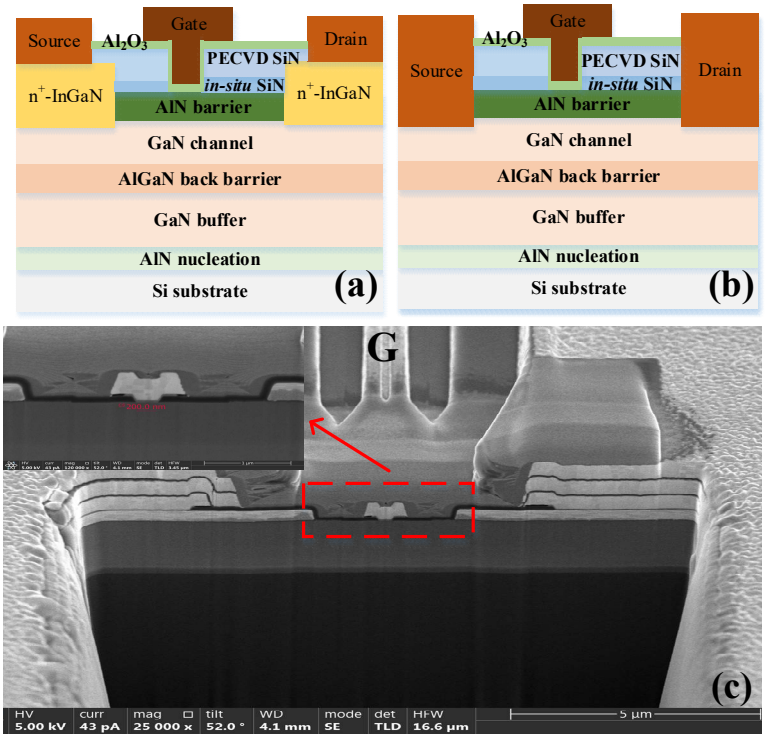

Fig. 1. (a) and (b) Schematic structure of Al_2O_3/AlN/GaN MOS-HEMTs on Si substrate with regrown ohmic contacts and alloyed ohmic contacts. (c) Cross-section SEM image of MOS-HEMTs. The inset gives the enlarged view of T-gate.

B-Appendix

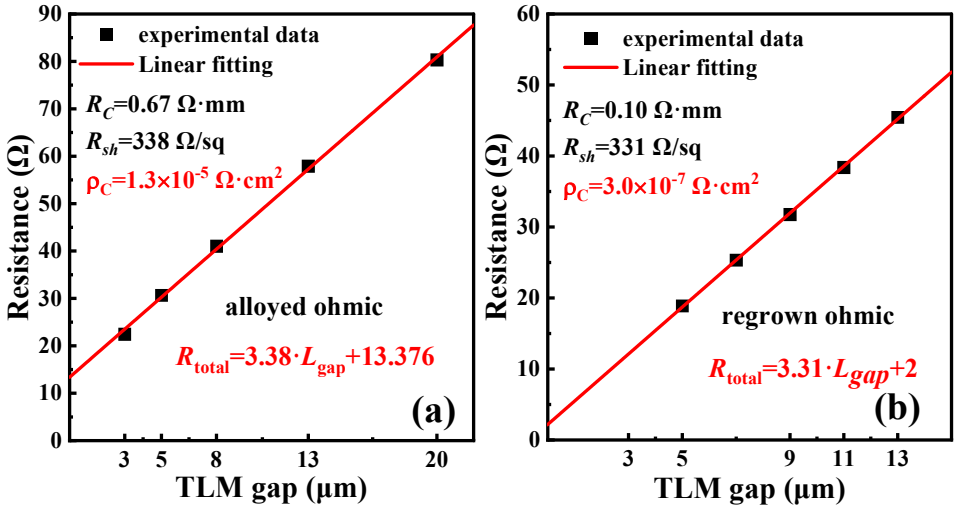

Fig. 2. (a) Alloyed and (b) regrown ohmic contact resistances extracted by transmission line method (TLM).

C-Appendix

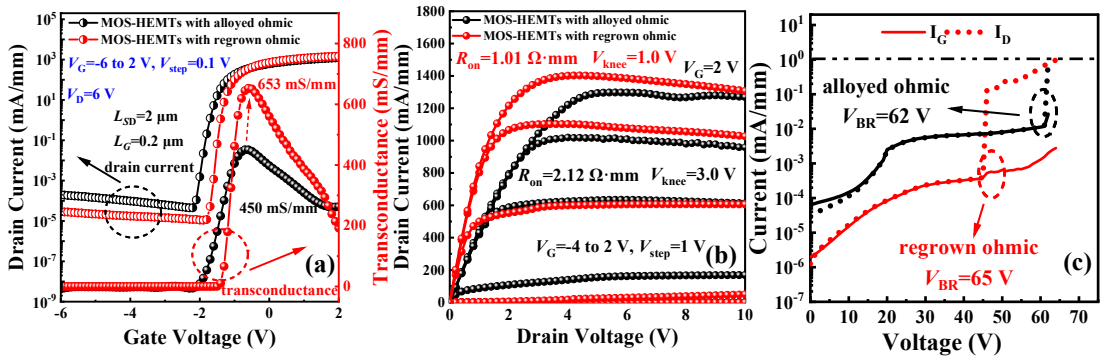

Fig. 3. (a) Transfer and (b) Output characteristics of MOS-HEMTs on Si. Black and red curves represent the devices with alloyed and regrown ohmic contacts, respectively. (c) Breakdown characteristics of MOS-HEMTs with regrown ohmic contacts and alloyed ohmic contacts.

D-Appendix

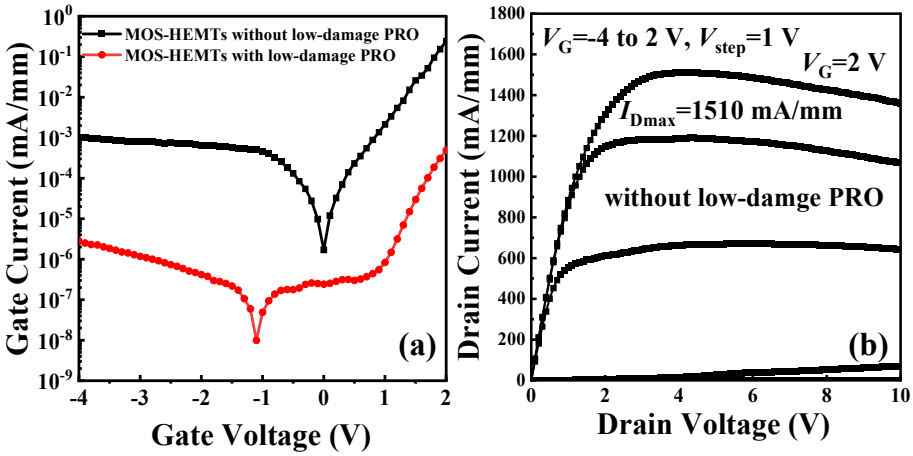

Fig. 4. (a) Schottky characteristics of MOS-HEMTs on Si. Black and red curves represent the devices without/with low-damage PRO treatment, respectively. (b) Output characteristics of MOS-HEMTs without low-damage PRO treatment.

E-Appendix

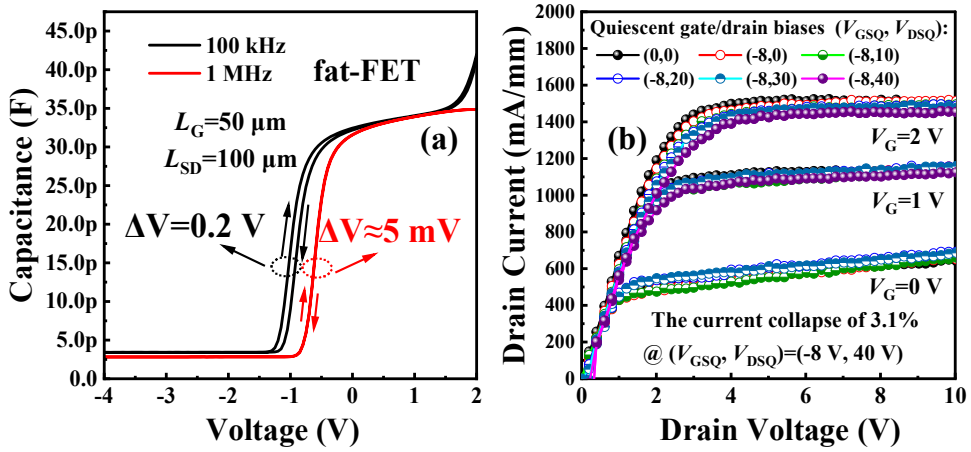

Fig. 5. (a) The *C-V* hysteresis curves and (b) Current collapse characteristics of MOS-HEMTs with regrown ohmic.

F-Appendix

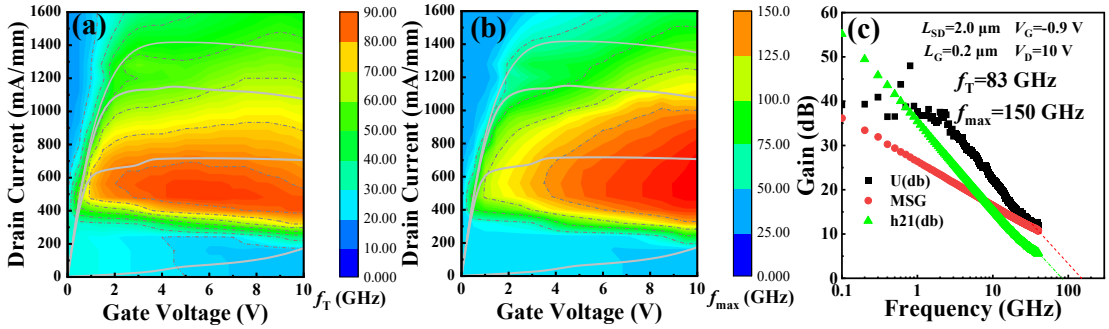

Fig. 6. (a) f_T and (b) f_{max} contour plots of Al_2O_3/AlN/GaN MOS-HEMTs on Si with regrown ohmic contacts. (c) Small-signal characteristics of 0.2-μm gate MOS-HEMTs measured at V_D=10 V.

G-Appendix

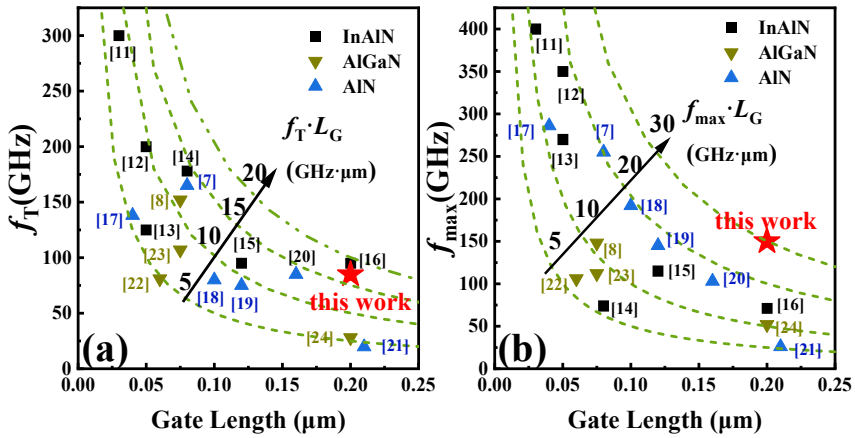

Fig. 7 Frequency benchmarks for GaN-on-Si HEMTs: (a) f_T versus L_G and (b) f_{max} versus L_G.